Inelastic Neutron Scattering Spectrum of Cyclotrimethylenetrinitramine: A Comparison with Solid-State Electronic Structure Calculations

Jennifer A. Ciezak* and S. F. Trevino

U.S. Army Research Laboratory, Weapons and Materials Research Directorate, Aberdeen Proving Ground, Maryland 21005

Received: December 6, 2005; In Final Form: February 23, 2006

Solid-state geometry optimizations and corresponding normal-mode analysis of the widely used energetic material cyclotrimethylenetrinitramine (RDX) were performed using density functional theory with both the generalized gradient approximation (BLYP and BP functionals) and the local density approximation (PWC and VWN functionals). The structural results were found to be in good agreement with experimental neutron diffraction data and previously reported calculations based on the isolated-molecule approximation. The vibrational inelastic neutron scattering (INS) spectrum of polycrystalline RDX was measured and compared with simulated INS constructed from the solid-state calculations. The vibrational frequencies calculated from the solid-state methods had average deviations of 10 cm^{-1} or less, whereas previously published frequencies based on an isolated-molecule approximation had deviations of 65 cm^{-1} or less, illustrating the importance of including crystalline forces. On the basis of the calculations and analysis, it was possible to assign the normal modes and symmetries, which agree well with previous assignments. Four possible "doorway modes" were found in the energy range defined by the lattice modes, which were all found to contain fundamental contributions from rotation of the nitro groups.

Introduction

In recent years, there has been considerable effort in obtaining a detailed understanding of detonation phenomena of energetic materials at a microscopic level. Of particular interest to the energetic materials community is the mechanism through which energy is transferred from a shock wave to the internal degrees of freedom. The exact pathway through which the mechanical energy of the shock wave is transferred is quite debatable, and several theories have been published that propose mechanisms through either electronic or vibrational paths.[1,2] Vibrational up-pumping is one vibrational theory where the energy generated from the shock wave is channeled from the lattice phonon vibrations into the internal molecular vibrations through a series of anharmonic couplings.[3] As the shock front propagates through the crystal, excess thermal and mechanical energy is transmitted into the phonon lattice modes. Anharmonic coupling of these phonon lattice modes with the internal vibrational modes provides a "doorway" for energy transfer to the upper vibrational states of the molecule, which eventually leads to molecular dissociation.[4]

Before the anharmonic coupling between the lattice and internal modes can be fully understood and applied to detonation theory, a fundamental knowledge of both the lattice and internal vibrational modes must be firmly established. In many cases, since theoretical models are increasingly being employed as a method to study shocked systems, obtaining accurate theoretical vibrational representations is also desired. In this paper, we investigate the vibrational properties of the widely used energetic material cyclotrimethylenetrinitramine (RDX) shown in Figure 1, using the experimental spectroscopic technique of inelastic neutron scattering and solid-state quantum chemical calculations.

Vibrational spectroscopy has been extensively used in the past to investigate the structural details and dynamical interactions of energetic materials.[4,5] However, this information is often incomplete either due to instrumental or method-based limitations, such as symmetry based selection rules. Direct comparisons of optical spectroscopic results to theory are often complicated because rarely is the nature of the electronic response entirely a function of the molecular motions. Inelastic neutron scattering is a vibrational spectroscopic technique, conceptually similar to Raman scattering, which is an attractive alternative to optical based spectroscopy and ideal for probing low frequency vibrational modes in materials. Because neutrons interact primarily with the atomic nuclei, rather than the electrons, the nature of the interaction is rather straightforward to model, allowing direct correlation of theoretical models with experimental data.[6] As such, vibrational INS spectra can be directly calculated from the mass-weighted normal mode hydrogen eigenvectors given as standard quantum chemical output. This combined experimental/theoretical approach has been developed extensively over the past decade and has generated considerable success in interpreting vibrational spectra.[7] These investigations have indicated density functional theory (DFT) calculations to be the most reliable in simulating experimental vibrational spectra.

RDX is a secondary explosive widely used both in civilian and military applications. The crystal structure of the ambient condition polymorph is well established using both X-ray[8] and neutron diffraction.[9] The structural data of RDX is supported by spectroscopic measurements, with both Raman[11] and infrared[10] results indicating the presence of a ring chair conformation with one nitro group in the equatorial position and the remaining two in the axial position. Computational studies have demon-

* To whom correspondence should be addressed. Address: Carnegie Institution of Washington, Geophysical Laboratory, 5251 Broad Branch Rd. N. W., Washington, DC 20015-1305. Tel: (202) 478-8953. E-mail: jciezak@arl.army.mil.

10.1021/jp057098u This article not subject to U.S. Copyright. Published 2006 by the American Chemical Society
Published on Web 03/24/2006

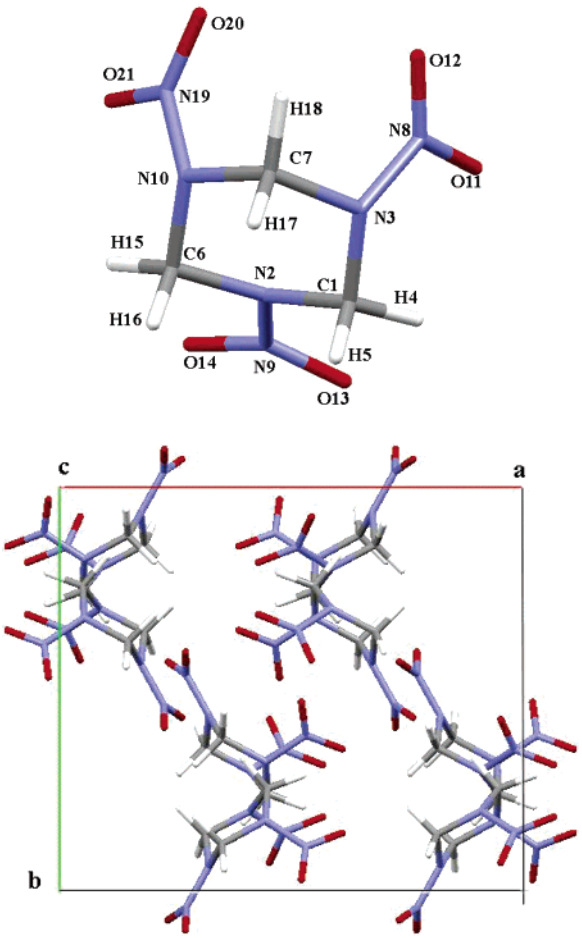

Figure 1. Molecular structure of the RDX molecule. An isolated molecule is shown at the left, and the crystal structure is shown at the right.

strated that an isolated-molecule approximation using the B3LYP/6-311+G** method yields an optimized geometry comparable to the neutron diffraction crystallographic analysis.[9] In addition, it has been shown that the DFT simulated infrared frequencies of RDX are in better agreement with solid-state experimental values than corresponding MP2 frequencies.[12] Despite this, the DFT gas-phase vibrational frequencies obtained from the isolated-molecule calculations do show significant deviation from the experimental IR and Raman data. As such, it seems warranted to obtain solid-state quantum chemical vibrational calculations. Solid-state calculations, while limited in the harmonic $k = 0$ approach, can provide a more accurate representation of the crystalline environment. These calculations are more accurate due to proper inclusion of crystal packing forces, intra- and intermolecular molecular hydrogen bonding interactions, as well as appropriate restrictions of the molecular motion within the crystal. Motivated by our past success in modeling inelastic neutron scattering spectra using solid-state DFT methods,[13] we have carried out an experimental INS study in conjunction with solid-state DFT calculations of RDX, with three primary goals: (1) to obtain a detailed understanding of how well the experimental vibrational spectrum is reproduced by the solid-state methods; (2) to look for possible "doorway modes" in the low-frequency region; and (3) to examine what effect, if any, anharmoncity has on the vibrational frequencies.

Materials and Methods

Experimental Methods. Inelastic neutron scattering data was collected with the filter analyzer neutron spectrometer (FANS) located at BT-4 at the National Institute of Standards and Technology Center for Neutron Research.[14] A detailed description of the FANS instrument including instrumental specifics has been presented.[15] The RDX sample was obtained from Picatinny Arsenal and recrystallized in acetone three times to remove impurities, such as HMX, prior to the experiment. Approximately 1 g of polycrystalline RDX was ground into a fine powder and loaded into an aluminum sample can. The sample can was then placed in a closed cycle helium refrigerator to maintain a constant temperature of 15 K for the duration of the experiments. The background contribution to the experimental spectrum caused by high-energy neutrons was obtained by scanning the sample cell with the detectors covered. The experimental spectrum was then normalized with respect to the background contribution using the data analysis and visualization environment (DAVE) program.[16]

Computational Methods. Solid-state quantum chemical calculations of RDX were performed with the DMol^3 package[17] using the SGI Origin Array located at the Wright Patterson Aeronautical Systems Major Shared Resource Center. Unit cell parameters and molecular geometry determined from room-temperature neutron diffraction[9] were obtained from the Cambridge Crystallographic Database and are as follows: Space group *Pbca*, $a = 13.182$ (2) Å, $b = 11.574$ (2) Å, $c = 10.709$ (2) Å, $Z = 8$. Calculations were performed using the generalized gradient approximation density functionals BLYP[17] and BP[18] functionals. The local density approximation functionals PWC[19] and VWN[20] were also tested. The "dnp" double-numeric basis set, which includes both d and p orbital polarization functions, and "fine" grid spacing were used in all calculations. Geometry optimizations were performed with no symmetry constraints and were continued until the energy difference between iterations was less than 10^{-6} a.u. Following geometry optimization, the Hessian matrix was constructed from the final optimized crystalline geometry for each theoretical method through finite differences of the analytic gradient. All solid-state vibrational frequencies presented are unscaled.

Theoretical INS spectra were constructed from the normal mode energies and eigenvectors using the A-Climax program v. 5.1.3.[21] The absolute intensities of the fundamental, combination, and overtone vibrations were calculated and averaged over all orientations of the momentum transfer. The determination of the intensity of each vibrational transition was based on the square of the hydrogen displacement, which was then weighted by the neutron scattering cross sections.

Results and Discussion

Molecular Geometry. Crystallographic[9] and calculated structural parameters of the RDX molecule are presented in Table 1. The atomic labeling in Table 1 is consistent with the numbering scheme presented in Figure 1. Table 1 presents the bond lengths first, followed by values for the root-mean square (RMS) standard deviations of the calculated values relative to the RDX crystal structure.[9] Several angles of the RDX molecule are also presented in Table 1, with the remaining angles reported in Table 1 of the Supporting Information.

A general comparison of the isolated-molecule and solid-state RDX molecular structures reveals the relatively small effect of the crystalline forces on the geometry. In comparison to experiment, the average RMS deviations of the bond lengths generated from the solid-state methods is at 0.019 Å, only slightly smaller than the 0.022 Å average RMS deviation generated from the isolated-molecule methods. Table 1 shows an interesting trend between the experimental neutron diffraction

TABLE 1: Isolated-Molecule and Solid-State Structural Parameters for RDX

bond (Å)	BLYP/dnp	BP/dnp	PWC/dnp	VWN/dnp	MP2/6-31G*[a]	B3LYP/6-31G*[a]	B3LYP/6-311+G**[a]	exp[b]
C1−N2	1.474	1.463	1.446	1.449	1.470	1.473	1.475	1.464
C1−N3	1.462	1.453	1.439	1.438	1.448	1.449	1.449	1.443
C7−N3	1.475	1.463	1.447	1.448	1.462	1.462	1.463	1.468
C7−N10	1.475	1.464	1.447	1.448	1.462	1.462	1.463	1.458
C6−N10	1.465	1.453	1.438	1.438	1.448	1.449	1.449	1.440
C6−N2	1.465	1.463	1.447	1.448	1.470	1.473	1.475	1.450
C1−H4	1.094	1.096	1.109	1.110	1.100	1.099	1.097	1.058
C1−H5	1.085	1.087	1.099	1.099	1.085	1.084	1.083	1.092
C7−H17	1.090	1.092	1.106	1.106	1.086	1.085	1.084	1.085
C7−H18	1.086	1.087	1.096	1.096	1.094	1.094	1.092	1.087
C6−H15	1.085	1.088	1.100	1.100	1.100	1.099	1.097	1.088
C6−H16	1.096	1.097	1.112	1.111	1.085	1.084	1.083	1.075
N2−N9	1.380	1.371	1.355	1.355	1.411	1.402	1.405	1.351
N3−N8	1.404	1.425	1.405	1.405	1.437	1.432	1.434	1.392
N10−N19	1.409	1.419	1.396	1.397	1.436	1.432	1.433	1.398
N9−O13	1.207	1.238	1.228	1.227	1.236	1.226	1.220	1.209
N9−O14	1.244	1.244	1.232	1.232	1.236	1.226	1.220	1.233
N8−O11	1.200	1.233	1.223	1.223	1.232	1.220	1.214	1.203
N8−O12	1.200	1.231	1.221	1.221	1.232	1.221	1.215	1.207
N19−O20	1.200	1.232	1.222	1.222	1.232	1.220	1.214	1.201
N19−O21	1.224	1.236	1.226	1.226	1.232	1.221	1.215	1.205
RMS	0.016	0.020	0.019	0.019	0.025	0.021	0.021	

angles (°)	BLYP/dnp	BP/dnp	PWC/dnp	VWN/dnp	MP2/6-31G*[a]	B3LYP/6-31G*[a]	B3LYP/6-311+G**[a]	exp[b]
θ_1	53.1	54.3	53.3	53.8	54.1	50.1	50.9	53.3
θ_2	43.6	44.3	43.8	44.3	42.7	41.4	41.4	43.7
δ	−12.8	−13.7	−12.4	−13.1	−27.9	−24.4	−24.1	−12.6

[a] Reference 12. [b] Reference 9.

structure[9] and the bond lengths generated from the local density functionals (PWC/dnp and VWN/dnp) and the nonlocal density functionals (BLYP/dnp, BP/dnp, B3LYP/6−31**, and B3LYP/6-311+G**). In general, the nonlocal methods overestimate the lengths of the nitrogen containing bonds by 5−10%,whereas the local methods tend to slightly underestimate the lengths of nitrogen-containing bonds by 2−5%. Both the isolated-molecule and solid-state calculations overestimate the N−N bonds by 2−7% and also the C1−H4 bond by 3−6%.

In the solid-state crystal calculations, there is evidence for the existence of a system of weakly interacting intramolecular hydrogen bonds. These bond lengths, which are summarized in Table 2 of the Supporting Information, range from 2.25 to 2.41 Å and are similar to the lengths of other weak hydrogen bonds in organic molecular crystals.[22] A slight rotation of the nitro groups brings each oxygen atom into closer proximity to the corresponding hydrogen atom. The LDA calculations show smaller hydrogen bonding distances than the GGA calculations, which is in better agreement with crystallographic experimental evidence. Extremely short C··O distances in the neutron diffraction experiment indicates the existence of strong networks of both intramolecular and intermolecular hydrogen bonds.[9−12,23] Close intermolecular contacts ranging from 2.34 to 2.46 Å are indicated in the solid-state calculations and are summarized in Table 2 of the Supporting Information.

Crystal structure analysis of RDX at room temperature determined the N2−NO_2 group to be essentially coplanar, whereas the N3−NO_2 and N10−NO_2 groups are slightly bent.[9] Table 1 presents a comparison of the θ_1, θ_2, and δ angles generated from the several theoretical methods[12] as well as neutron diffraction.[9] The angle between the C1−N3−N10−C6 and C1−N2−C6 planes has been designated θ_1, and the angle between the planes containing N3−C7−N10 and C1−N3−N10−C6 has been labeled θ_2. The δ angle refers to the tilt of the N−N bond away from the CNC plane.[12] All solid-state methods used in this report have an average θ_1 and θ_2 deviation ranging between 0% and 2.5%. The calculations based on the isolated-molecule approximation have an average θ_1 and θ_2 deviation from experimental values between 1 and 6%.[12] The RMS values of the δ angle calculated using the solid-state methods range from 3.2 to 8.8%, with the PWC/dnp results giving the best comparison to experiment and the BP/dnp the worst. In contrast, the methods based on the isolated-molecule approximation have deviations of 11.5 − 15.3°.

Experimental and Simulated Spectra

The results of the solid-state normal modes analyses are shown in conjunction with the experimental inelastic neutron scattering spectrum in Figure 2 and are summarized in Table 2. Each simulated spectra shown in Figure 2 presents the fundamental vibrations as well as the combination and overtone vibrational modes. Figure 2 shows that the relative intensities of the fundamental calculated inelastic neutron scattering peaks are generally in good agreement with the relative intensities of the experimental peaks. This is a strong indication that using the calculated normal mode eigenvectors that involve hydrogen motion to represent the entire vibrational motion of the RDX molecule within the crystal is a good approximation to the experimental vibrational dynamics. In contrast to the good intensity agreement of the fundamental vibrations with experiment, the intensities of the simulated combination and overtones vibrations are underestimated in all spectra. This result is not surprising, however, because the intensities of these vibrations are strongly dependent on the intensities of the fundamental vibrations, and even relatively small errors in the calculated fundamental intensities can have a large effect on the intensities of the combination and overtone vibrational modes.

Table 2 presents a comparison of the experimentally observed as well as both of the solid-state and isolated-molecule[12] calculated frequencies of RDX. In addition, frequencies obtained from optical spectroscopic methods are shown.[10,11] Molecular symmetry assignments are based on the nearly C_s symmetry in the solid.[9] These symmetry assignments, while valid for the

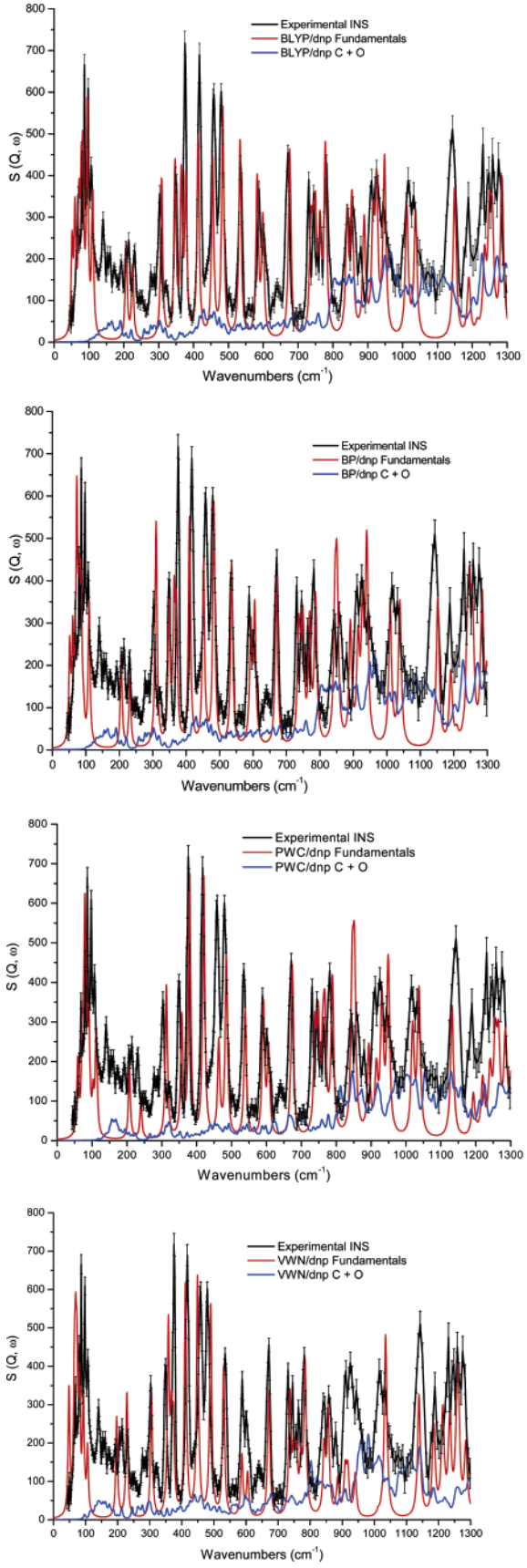

Figure 2. Comparison of the inelastic neutron scattering spectrum (15 K) of RDX and the solid-state calculations using the (top to bottom) BLYP/dnp, BP/dnp, PWC/dnp, and VWN/dnp methods. Shown in each plot are the experimental spectrum (black trace), the calculated fundamental vibrations (red trace), and the combinations and overtone vibrations (blue trace).

isolated-molecule calculations, are not entirely correct for the solid-state calculations, where one must also account for the D_{2h} factor group symmetry. However, to make a valid comparison between the isolated-molecule calculations and solid-state calculations, the factor group symmetry is being neglected.

Table 2 shows that, in most cases, the calculated frequencies generated from the both the LDA and GGA solid-state methods are within 10 cm^{-1} or less of the experimental frequencies. The average RMS difference between the experimental INS frequencies and the corresponding BLYP/dnp calculated frequencies is 4.47 cm^{-1}. This RMS value slightly increases in both the BP/dnp and PWC/dnp to 5.13 and 6.11 cm^{-1}, respectively. The average RMS difference between the experimental INS and corresponding VWN/dnp calculated frequencies is 4.82 cm^{-1}. In contrast, the RMS values of the MP2/6-31G* and B3LYP/6-311+G** calculations are 63.53 and 46.54 cm^{-1}, respectively.[9] Although the low RMS values of the solid-state calculations partially stem from the relatively accurate molecular geometry, it is evident that inclusion of the crystal cell interactions result in significantly improved frequency agreement with the experimental INS spectrum. The inclusion of the crystal packing forces is an important factor in determining the correct vibrational frequencies of cyclic, flexible molecules, but in the RDX case, several intermolecular interactions between neighboring molecules have been shown to exist. These interactions can have a large effect on the intramolecular interactions of the isolated molecule and, although not noticeably effecting the molecular geometry, lead to substantial changes in the vibrational frequencies.

The low frequency vibrational region of the inelastic neutron scattering spectrum is shown in Figure 3 and summarized in both Tables 2 and 3. In this experimental spectrum, several well-resolved vibrational modes are observed atop a broad phonon band. At the very edge of the broad band is a barely resolvable sharp peak at 50 cm^{-1} that may be attributed to the NO_2 wag of the axial groups with A′ symmetry. The exact assignment of this mode is somewhat questionable because it has been previously assigned as phonon mode using Raman spectroscopy.[24] The intense INS feature observed at 69 cm^{-1} can be labeled as a wag of the axial nitro groups. The signal-to-noise ratio in the range of 70−75 cm^{-1} is only good enough to imagine a vibrational transition centered at 74 cm^{-1} which could be assigned to the axial NO_2 wag. The strong vibrational intensity of the mode ca. 79 cm^{-1} is due to simultaneous rotation of the nitro groups. Neither the mode at 74 cm^{-1} nor the mode at 79 cm^{-1} have been observed using optical spectroscopy. The experimental vibrational band at 86 cm^{-1} can be assigned as rotation of the equatorial nitro groups. Two modes are experimentally observed at 97 and 107 cm^{-1}, which could be assigned to a molecular bending vibration coupled with rotation of the nitro groups.

Several of the vibrational modes discussed above are in close proximity to previously assigned lattice modes at 50, 59, 72, 86, and 102 cm^{-1}.[24] The vibrational intensities of these transitions were not given in the report,[24] but it is possible to suggest the existence of several of these modes through close examination of the experimental INS spectrum of Figure 3. A broad vibration of low intensity is observed at approximately 48 cm^{-1}, which may be the previously assigned lattice vibration ca. 50 cm^{-1}. At 58 cm^{-1}, another low intensity broad vibration is observed that may be the 59 cm^{-1} mode. The intense vibration observed at 110 cm^{-1} appears to have a slight shoulder that may be due to the 102 cm^{-1} lattice mode. The vibrational intensity is too weak to determine the existence of a vibration

TABLE 2: Experimental and Calculated Vibrational Frequencies[a]

	INS	Raman[b]	IR[b,c]	BLYP/ dnp	BP/ dnp	PWC/ dnp	VWN/ dnp	MP2/ 6-31G*[d]	B3LYP/ 6-311+G**[d]	symmetry	molecular motion
1	50			52	52	59	48	37	44	A′	NO_2 wag (ax)
2	69			60	61	72	65	60	60	A	NO_2 wag (eq)
3	74			72	73	79	69	65	63	A	NO_2 wag (ax)
4	79			78	80	84	73	67	74	A′	NO_2 rot. (all)
5	86			83	86	91	81	86	93	A′	NO_2 rot. (eq)
6	97	90		90	93	103	93	137	107	A	NO_2 rot. (ax)
7	107	106	104	111	110	112	106	217	209	A′	molecular bend + NO_2 rot. (all)
8	205	205	208	207	206	207	197	250	229	A	N−NC_2 umb. (eq) + NO_2 rot. (ax)
9	230	224	223	225	232	240	229	293	290	A′	ring rot. + NO_2 rot. (all)
10	305			308	310	313	305	336	325	A	molecular st.
11	351	347	345	347	349	357	358	398	371	A′	ring twist
12	373			365	364	379	368	432	403	A′	N−NC_2 umb. (ax. Carbons)
13	375			378	371	380	374	434	406	A	ring bend (flattening)
14	416	414	410	413	410	420	411	482	438	A′	ring bend (folding)
15	459	463	461	455	452	463	449	512	463	A′	ring bend (folding) + N−N st. (ax)
16	482	486	486	484	483	485	490	577	579	A	ring twist + NO_2 rock (eq)
17	535			534	536	539	530	592	588	A	ring twist
18	590	588	589	583	593	591	587	618	610	A′	ring bend
19	602	605	602	599	605	606	605	657	651	A	ring rock
20	671	669	670	676	670	674	671	675	676	A′	ring bend
21	734	739	738 (739)	737	736	739	737	740	756	A	N−NO_2 umb. (ax)
22	744			744	741	748	749	756	761	A′	N−NO_2 umb. (ax)
23	755			750	749	762	757	766	769	A	N−NO_2 umb. (eq)
24	763	756	755	763	769	767	771	803	803	A	ring bend + NO_2 sci.
25	782	786	783 (782)	778	787	789	784	859	855	A	C−N st. + NO_2 sci. (eq)
26	843	847	844 (844)	841	845	846	845	864	870	A′	N−N st + NO_2 sci. (ax)
27	857	855	853 (853)	853	851	852	856	912	896	A	C−N st. + N−N st. (ax)
28	880	884	883 (883)	890	891	893	886	954	909	A′	C−N st. + CH_2 rock + N−N st.
29	911		915 (915)	915	914	915	909	967	937	A	ring breathing
30	925	920	926 (925)	925	927	931	917	979	951	A	CH_2 rock + N−N (eq) st.
31	944	943	947 (947)	948	940	949	940	1040	1011	A	N−N st. (eq) +CH_2 twist + CH_2 rock
32	1015		1019 (1019)	1012	1010	1019	1011	1069	1036	A′	CH_2 rock + CH_2 twist
33	1032	1029	1040 (1039)	1037	1039	1037	1035	1195	1153	A′	N−C st.
34	1143		(1143)	1149	1152	1132	1139	1246	1230	A	CH_2 rock
35	1188		(1181)	1190	1191	1193	1185	1272	1238	A′	N−C st.
36	1215	1214	1219 (1218)	1214	1209	1220	1213	1294	1264	A	N−C st.
37	1231	1232	(1234)	1235	1241	1241	1235	1305	1270	A′	CH2 tw.
38	1251			1249	1247	1256	1256	1320	1296	A	N−N st. (ax) + O−N−O st. + H−C−H wag
39	1258			1257	1256	1265	1261	1322	1299	A′	N−N st. (ax)
40	1275	1273	1275 (1268)	1285	1285	1285	1285	1365	1337	A	CH_2 twist + N−N st. (ax)
RMS				4.48	5.13	6.11	4.82	63.53	46.54		

[a] Symmetry assignments are shown and a brief description of the molecular motion is included. Values of the second IR study are presented in parentheses. [b] Reference 11. [c] Reference 10. [d] Reference 12.

at approximately 72 cm^{-1}. Better spectral resolution and signal-to-noise ratio is needed before the positions of these modes can be considered absolute. In addition, two overtones of the lattice modes, which have been reported at 33 and 48 cm^{-1} [11] are observed in the INS spectrum at 63 and 96 cm^{-1}.

The spectral region between 100 and 300 cm^{-1} is especially interesting because "doorway modes" are reported to fall in this general spectral range.[3] These vibrations, which arise from combination of a phonon lattice mode and fundamental vibration are widely thought to only occur from the energy range defined by the first overtone of the lowest energy lattice mode of lowest energy to the first overtone of the highest energy lattice mode. Rey-Lefon[11] observed the phonon energy range to be between 20 and 74 cm^{-1} making the range of "doorway modes" between 40 and 148 cm^{-1}. Within this range, four vibrations are observed at 101, 133, 140, and 145 cm^{-1}. It is rather interesting to note that these four modes all have fundamental counterparts that consist of rotation of the NO_2 groups. This is particularly important because it has been proposed that the initial bond broken in detonation is the N−N bond that connects the nitro group to the peripheral molecule.[25] Surprisingly, there are also

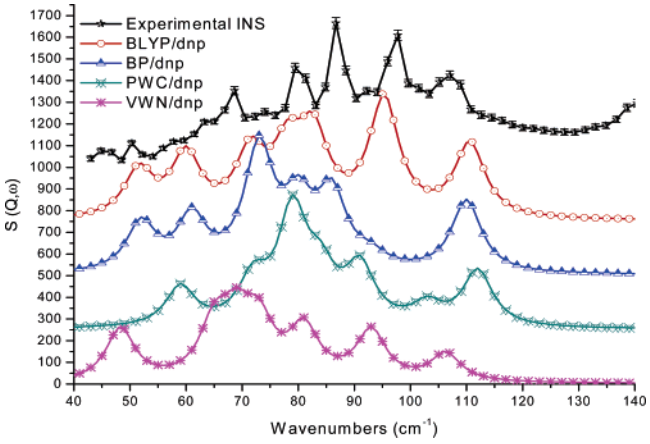

Figure 3. Comparison of the experimental low frequency inelastic neutron scattering spectrum (black trace) to the simulated inelastic neutron scattering spectra obtained from the BLYP/dnp (red trace, circle), BP/dnp (blue trace, triangle), PWC/dnp (green trace, crossed triangle), and VWN/dnp (pink trace, asterisk) methods. All spectra are arbitrarily scaled for clarity.

TABLE 3: Experimental and Calculated Lattice, Combinations, and Overtones Vibrational Modes from 40 to 300 cm^{-1}[a]

INS	BLYP/dnp	BP/dnp	PWC/dnp	VWN/dnp	assignment
48	50	51	48	48	lattice mode
58	60	59	60	59	lattice mode
63	62	63	62	65	first overtone 33 cm^{-1} lattice mode[b]
96	100	102	96	94	first overtone 48 cm^{-1} lattice mode
101	101	103	106	95	79 cm^{-1} + 22 cm^{-1} lattice mode[b]
133	133	137	139	129	86 cm^{-1} + 48 cm^{-1} lattice mode
140	143	142	144	138	107 cm^{-1} + 33 cm^{-1} lattice mode[b]
145	144	145	142	140	86 cm^{-1} + 58 cm^{-1} lattice mode
153	150	153	163	142	74 cm^{-1} + 79 cm^{-1}
159	156	160	168	146	first overtone 79 cm^{-1} mode
161	155	159	170	151	86 cm^{-1} + 74 cm^{-1}
172	162	166	182	162	97 cm^{-1} + 74 cm^{-1}
183	183	183	191	175	107 cm^{-1} + 86 cm^{-1}
192	194	196	203	187	86 cm^{-1} + 107 cm^{-1}
196	180	186	206	186	first overtone 97 cm^{-1} mode
214	222	220	224	212	first overtone 107 cm^{-1} mode
239	239	238	239	229	205 cm^{-1} + 33 cm^{-1} lattice mode[b]
253	257	257	255	245	205 cm^{-1} + 48 cm^{-1} lattice mode
261	272	271	272	260	214 cm^{-1} + 48 cm^{-1} lattice mode ?
270	272	276	287	260	192 cm^{-1} + 79 cm^{-1} ?
274	267	267	279	262	205 cm^{-1} + 69 cm^{-1}
278	279	279	286	266	205 cm^{-1} + 74 cm^{-1}
281	277	284	299	277	230 cm^{-1} + 50 cm^{-1}
288	285	291	289	299	230 cm^{-1} + 58 cm^{-1} lattice mode
296	284	290	324	282	50 cm^{-1} + 246 cm^{-1} ?

[a] Assignment shown with a question mark indicates an unclear assignment. [b] The vibrational frequencies of these lattice modes were obtained from ref 11.

four other possible doorway modes above the 148 cm^{-1} cutoff range, although one assignment is questionable. These vibrations at 239, 253, 261 (questionable assignment), and 288 cm^{-1} may be accidental couplings, but since they also involve fundamental vibrations which have nitro group rotation, it seems likely these are, in fact, additional "doorway modes". These additional modes may be a reason for the increased sensitivity of RDX relative to other energetic materials, but further work will be required to reach any definite conclusions.

The low frequency region of the vibrational spectrum is also important from the viewpoint of judging how anharmonic the system is at 15 K. Typically, varying the temperature and charting the vibrational shifts is used to measure the degree of anharmocity. However, it is possible to obtain a rough estimate of the degree of anharmonicity of the system by comparing the experimentally determined combination and overtone modes with those constructed from the harmonic solid-state calculations. If there is a significant degree of anharmonicity, one would expect the experimental and calculated modes to differ significantly, since our calculated combination and overtone modes are simply constructed from sums, differences, and multiples of the fundamental bands. Table 3 presents a comparison of the combination modes observed in the region from 48 to 300 cm^{-1}. In general, the GGA functionals, BLYP/dnp and BP/dnp, have slightly better agreement with experiment with RMS values of 6.13 and 4.71 cm^{-1}, respectively. (Note that these RMS values omit the first two modes, which are lattice modes.) The LDA functionals, PWC/dnp and VWN/dnp, have slightly larger RMS values of 10.31 and 8.49 cm^{-1}. The slight difference in the RMS values between the GGA and LDA functionals is not surprising considering the GGA functionals are better parametrized for organic hydrogen-bonded systems. Since the RMS values of the BLYP/dnp and BP/dnp fundamentals are comparable to the RMS values of the combinations and overtones, it seems safe to assume that little if any anharmonicity is reflected in the RDX system at 15 K. The "doorway modes" although reported to be highly anharmonic also do not reflect a significant degree of anharmonicity at this low temperature. It would be interesting to perform a systematic temperature scan of these modes, but that is currently beyond the scope of this paper.

Conclusion

The inelastic neutron scattering spectrum has been analyzed with solid-state density functional methods in addition to previously published isolated-molecule calculations. The inclusion of the crystalline environment, although not necessary to obtain the correct geometry, greatly improves vibrational agreement with experiment, relative to the isolated-molecule frequency values. The normal-mode assignments were made based on the solid-state results at the BLYP/dnp level of theory. Combinations, overtones and several lattice modes were assigned in the low-frequency region (45−300 cm^{-1}) in the interest of finding "doorway modes". There were four possible modes observed in the defined energy range of these vibrations, which for RDX is 40−148 cm^{-1}. All of these modes had a fundamental vibrational component consisting of rotation of one or more nitro groups. This point is rather important and supports the idea that the N−N bond is the initial bond broken in decomposition. In addition, there were combinations of fundamental and lattice modes found up to 288 cm^{-1}, which is well out of the energy range associated with "doorway modes". Although no definite conclusions can be made as to whether these couplings are simply coincidental or in fact "doorway modes", it is rather interesting to note that these modes also consist of fundamental vibrations with primarily nitro group rotation. Although "doorway modes" have been reported to be highly anharmonic, we found that our harmonic solid-state calculations were able to provide relatively accurate frequency values. This trend was also observed in other combination and overtone modes presented. The GGA functionals were found to have better RMS agreements for these modes than the LDA functionals and this may be simply because the GGA functionals are better parametrized for organic hydrogen bonded systems. Further investigations of the application of solid-state density functional theory to interpret INS spectra of other energetic materials are currently underway.

Acknowledgment. The authors acknowledge the NIST Center for Neutron Research for providing beamtime on the FANS instrument. The Wright Patterson Major Shared Resource Center is thanked for providing access to the DMol3 program. This work was supported by the Army Research Laboratory and part of the work was performed while J.C. was under a National Research Council Fellowship with ARL.

Supporting Information Available: Isolated-molecule and solid-state bond angles (Table 1) and inter- and intramolecular hydrogen bonding interactions (Table 2). This material is available free of charge via the Internet at http://pubs.acs.org.

References and Notes

(1) Satija, S. K.; Swanson, B.; Eckert, J.; Goldstone, J. A. *J. Phys. Chem.* **1991**, *95*, 10103.

(2) Dremin, A. N. *Toward Detonation Theory*; Springer-Verlag: New York, 1999.

(3) (a) Dlott, D. D.; Fayer, M. D. *J. Chem. Phys.* **1990**, *92*, 3798. (b) Kim, H.; Dlott, D. D. *J. Chem. Phys*. **1990**, *93*, 1695.

(4) Stevens, L. L.; Haycraft, J. J.; Eckhardt, C. J. *Cryst. Growth Des.* **2005**, *5*, 2060.

(5) See, for example: (a) Grudzdkov, Y. A.; Dreger, Z. A.; Gupta, Y. M. *J. Phys. Chem. A* **2004**, *108*, 6216. (b) McGrane, S. D.; Shreve, A. P. *J. Chem. Phys.* **2003**, *119*, 5834. (c) Torres, P.; Mercado, L.; Cotte, I.; Hernandez, S. P.; Mina, N.; Santana, A.; Chamberlain, R. T.; Lareau, R.; Castro, M. E. *J. Phys. Chem. B* **2004**, *108*, 8799. (d) Haussler, A.; Klapotke, T. M.; Holl, G.; Kaiser, M. *Prop. Exp. Pyro.* **2002**, *27*, 12. (e) Towns, T. G. *Spectrosc. Chim. Acta* **1983**, *A39*, 801.

(6) Hudson, B. S. *J. Phys. Chem. A* **2001**, *105*, 3949.

(7) See, for example: (a) Plazanet, M.; Fukushima, N.; Johnson, M. R. *Chem. Phys.* **2002**, *280*, 53. (b) Johnson, M. R.; Parlinski, K.; Natkaniec, I.; Hudson B. S. *Chem. Phys.* **2003**, *291*, 53. (c) Hudson, B. S.; Allis, D. G.; Parker, S. F.; Ramirez-Cuesta, A. J.; Herman, H.; Prinzbach, H. *J. Phys. Chem. A* **2005**, *109*, 3418. (d) Plazanet, M.; Fontain-Vive, F.; Gardner, K. H.; Forsyth, V. T.; Ivanov, A.; Ramirez-Cuesta, A. J.; Johnson, M. R. *J. Am. Chem. Soc.* **2005**, *127*, 6672. (e) Natkaniec, I.; Holderna-Natkaniec, K.; Majerz, I.; Parlinski, K. *Chem. Phys.* **2005**, *317*, 171.

(8) McCrone, W. *Anal. Chem.* **1950**, *22*, 954.

(9) Choi, C. S.; Prince, E. *Acta Crystallogr.* **1972**, *B28*, 57

(10) Karpowicz, R. J.; Brill, T. B. *J. Phys. Chem.* **1984**, *88*, 348.

(11) Rey-Lafon, M.; Trinque-Coste, C.; Cavagnat, R.; Forel, M.-T. *J. Chim. Phys. Chem. Biol.* **1971**, *68*, 1533.

(12) Rice, B. M.; Chabalowski, C. F. *J. Phys. Chem. A* **1997**, *101*, 8720.

(13) (a) Ciezak, J. A.; Trevino, S. F. *J. Mol. Struct. (THEOCHEM)* **2005**, *732*, 211. (b) Ciezak, J. A.; Trevino, S. F. *J. Mol. Struct. (THEOCHEM)* **2005**, *723*, 241. (c) Ciezak, J. A.; Trevino, S. F. *Chem. Phys. Lett.* **2005**, *403*, 329.

(14) Certain commercial software and instruments are identified in this paper to foster understanding. Such identification does not imply recommendation or endorsement by the National Institute of Standards and Technology, nor does it imply that the software or equipment identified are necessarily the best available for this purpose.

(15) (a) Copley, J. R. D.; Neumann, D. A.; Kamitakahara, W. A. *Can. J. Phys.* **1995**, *73*, 763. (b) Udovic, T. J.; Neumann, D. A.; Leão, J.; Brown, C. M. *Nucl. Instrum. Methods Phys. Res., Sect. A* **2004,** *517*, 189.

(16) http://www.ncnr.nist.gov/dave

(17) Delley, B. *J. Chem. Phys.* **1990**, *92*, 508.

(18) (a) Becke, A. D. *Phys. Rev.* **1988**, *A38*, 3098. (b) Perdew, J. P. *Phys. Rev.* **1986**, *B33*, 8822.

(19) Perdew, J. P.; Wang, Y. *Phys. Rev.* **1992**, *B45*, 13244.

(20) Vosko, S.; Wilk, L.; Nussair, M. *Can. J. Phys.* **1980**, *58*, 1200.

(21) Ramirez-Cuesta, A. J. *Comput. Phys. Comm.* **2004**, *157*, 226.

(22) Desiraju, G. R.; Steiner, T. *The Weak Hydrogen Bond In Structural Chemistry and Biology*; Oxford University Press: Oxford, U.K., 1999.

(23) Sorescu, D. C.; Rice, B. M.; Thompson, D. L. *J. Phys. Chem. B* **1997**, *101*, 798.

(24) Owens, F. J.; Iqbal, Z. *J. Chem. Phys.* **1981**, *74*, 4242.

(25) Luty, T.; Orden, P.; Eckhardt, C. J. *J. Chem. Phys.* **2002**, *117*, 1.